ACS APPLIED NANO MATERIALS

www.acsanm.org Article

Nanoscale Fluorinated Carbon Dots for the Detection of Perfluorooctanoic Acid in Aqueous Systems: A Fluorescence Assay Enhanced by Fluorophilic Interactions

Somayeh Mohammadi,* Zayra N. Dorado, and Hamidreza Sharifan*

Cite This: *ACS Appl. Nano Mater.* 2024, 7, 21410−21419 Read Online

ACCESS | Metrics & More | Article Recommendations | Supporting Information

ABSTRACT: Due to the growing demand for per- and poly fluoroalkyl substances (PFAS) detection, analytical methods are progressively focused on developing facile and efficient techniques for detecting PFAS compounds in water systems to eliminate the need for complex procedures. Here, we developed a nanoscale fluorine(F), nitrogen(N)-doped carbon dot-based fluorescence (FL) sensor designed for the sensitive detection of perfluorooctanoic acid (PFOA) in drinking water. To counterbalance the effects of the N/F ratio on fluorophilicity, the synthesis of fluorinated carbon dots (F-CDs) was optimized by examining polyethylenimine (PEI) to tetrafluoroterephthalic acid (TFTA) ratio from 1:3 to 1:10. The highest quantum yield of 10.6% was achieved at a 1:3 ratio. The F-CDs demonstrated a blue fluorescence with optimum excitation and emission wavelengths at 350 and 470 nm, respectively. F-CDs were extensively characterized using fluorine nuclear magnetic resonance (FNMR), Fourier transform infrared spectroscopy (FTIR), transmission electron microscopy (TEM), energy dispersive spectroscopy (EDS), X-ray diffraction (XRD), X-ray photoelectron Spectroscopy (XPS), dynamic light scattering (DLS), and ζ-potential measurements. ζ-Potential analysis confirmed the surface chemistry of the F, N-CDs, as evidenced by their cationic nature. The interaction with the PFOA led to a noticeable decrease in the surface charge of the CD, as evidenced by electrostatic, and fluorophilic interactions. The sensor exhibited high sensitivity and selectivity toward PFOA within the detection range from 10 to 1660 ppt and a low detection limit of 3 ppt. The sensor's capability to measure PFOA concentrations in groundwaters with high accuracy provides a reliable detection method for safeguarding water resources and public health, making it a valuable tool for environmental monitoring.

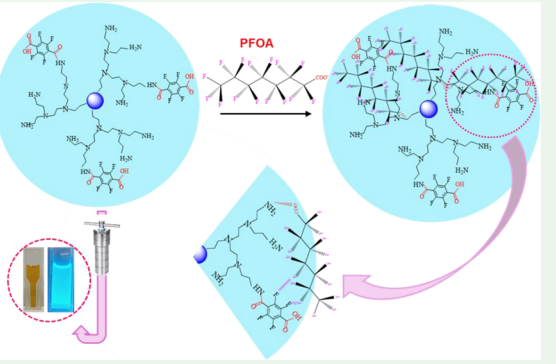

KEYWORDS: *fluorescence sensor, PFAS, environmental sensing, fluorinated carbon dots, fluorophilic Interactions, groundwater*

1. INTRODUCTION

Per- and polyfluoroalkyl substances (PFAS) represent a group of extremely persistent fluorinated organic contaminants with more than 10,000 diverse formulations.[1−4] PFAS analytes hold complex physiochemical structures, which lead to different degrees of classification including polarity, chain length, hydrophobicity, and surface charge. The amphiphilic nature of PFAS species has resulted in contamination of natural and engineering water systems.[5−7] Since 2016, the health advisory level for PFAS mother compounds of perfluorooctanoic acid (PFOA) and perfluorooctanesulfonic acid (PFOS) from 70 ng/L in drinking water reduced as low as 8 ng/L.[8,9] However, the critical challenge remains as the detection procedure and increasing demand for analysis which is highly limited, lengthy, and costly.[8] The primary detection technique[9,10] relies on the availability of liquid chromatography-tandem mass spectrometry (LC-MS/MS), a labor-intensive and expensive method. Young et al. applied the Fourier-transform ion cyclotron resonance mass spectrometry (FT-ICR MS) but was limited to a few national Laboratories worldwide.[3] Therefore, recent research has shifted toward developing alternative PFAS sensing technologies, including optical, electrochemical, and nanomaterial-based sensors, aiming for simpler, affordable, and quicker portable PFAS detections.[3,11,12] Among advanced sensors, fluorescence (FL)-driven sensors are the frontiers due to their versatility, low cost, and high sensitivity. These sensors are categorized into "turn-on"[13] and "turn-off"[14] types, indicating an increase or decrease in fluorescence in the presence of PFAS. The molecular interaction between the fluorescent probe and PFAS through electrostatic or hydrophobic forces in an aqueous system alters the light-emitting

Received: May 29, 2024
Revised: September 4, 2024
Accepted: September 5, 2024
Published: September 10, 2024

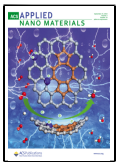

https://doi.org/10.1021/acsanm.4c03109
ACS Appl. Nano Mater. 2024, 7, 21410−21419

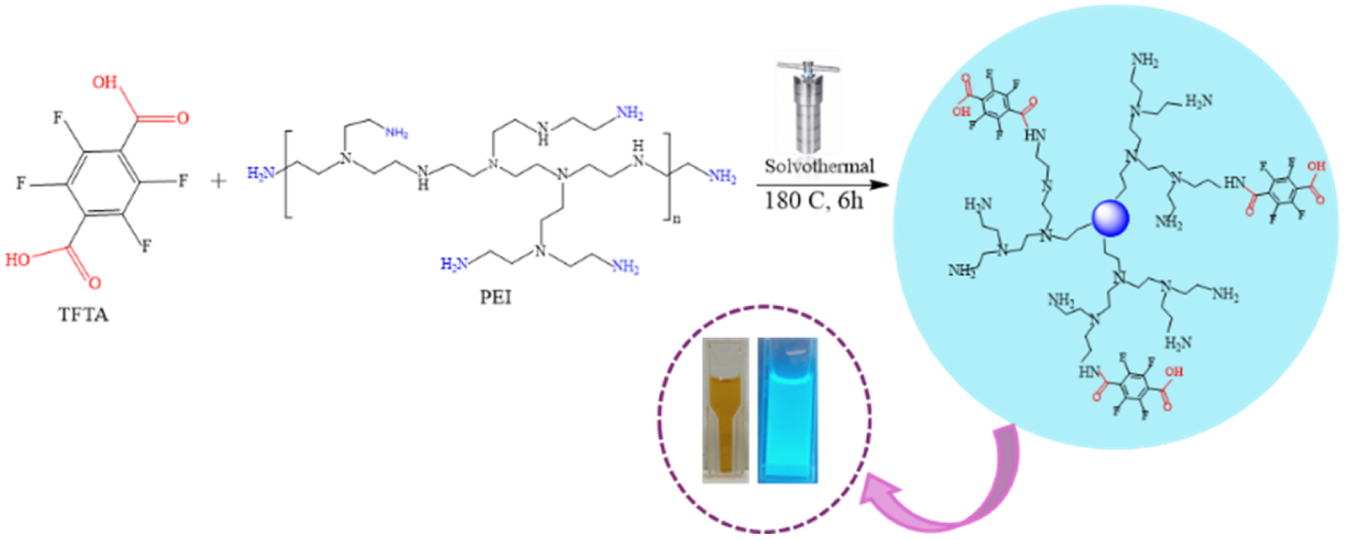

Figure 1. Schematic representation of the synthesis pathway for cationic and fluorine-rich carbon dots (CDs) used in PFAS detection.

characteristics, resulting in fluorescence changes corresponding to the PFAS concentration.[15]

Carbon dots (CDs) are photochemically stable nanomaterials with a high potential for the fluorescence-based detection of PFAS in water systems due to amorphous physics, organic nature, high emissivity, and cost-effectiveness.[16−19] The specific application targeted in this study is environmental monitoring, particularly detecting harmful PFAS compounds in drinking water to safeguard public health. Selecting appropriate precursors for nanoscale CD synthesis can be strategically designed to include hydrophobic regions and functional groups, facilitating electrostatic interactions.[17,20] C−F bonds in fluorinated compounds can engage in polar hydrophobic interactions, known as fluorophilic interactions.[21] This unique affinity allows for the effective binding of PFAS molecules. Previous research has shown that fluorinated compounds, such as highly fluorinated porous cyclodextrin polymers, can effectively capture PFAS like PFOA at environmentally relevant concentrations.[22] These findings emphasize that fluorine−fluorine interactions and electrostatic attractions are vital for the selective and efficient determination of PFAS from aqueous solutions.[23,24] Several nanoscale CD-based sensors have been reported for detecting PFOA and PFOS, utilizing electrostatic interactions. However, these sensors have encountered challenges with low sensitivity.[17,25−28] Merging fluorinated and cationic probes in one sensing system will amplify PFAS detection by utilizing synergistic effects between fluorophilic and electrostatic interactions.[11] This hypothesis was examined in this study by employing PEI, a polymer precursor abundant in positively charged amine groups, to enhance CD' electrostatic interactions, and by using TFTA to incorporate hydrophobic sites within the CDs.

Aiming for enhanced sensing capabilities and the development of a straightforward, rapid, economical, and sensitive PFAS detection technique, F-CDs were utilized as a fluorescence probe for PFOA quantification. These F-CDs were synthesized through a solvothermal method, employing TFTA as the F-donor and PEI to introduce sites of positive charge. The abundant positive nitrogen (N) sites from PEI enable the electrostatic attraction to PFOA. Concurrently, the presence of fluorine residues in the structure promotes a stronger probe affinity for PFOA through fluorophilic interactions. The effectiveness of this method was demonstrated through the analysis of groundwater samples, achieving recovery rates ≥90% and relative standard deviation (RSD) values of ≤7%, emphasizing its significance for environmental monitoring purposes.

2. EXPERIMENTAL SECTION

2.1. Reagents and Chemicals. TFTA, pentadecafluorooctanoic acid, pentadecafluorooctanoic acid (100 μg/mL methanol), quinine sulfate (used for quantum yield (QY) measurement), and ethanol were purchased from Sigma-Aldrich (MO). Terephthalic acid (TA) was obtained from TCI America (Portland, OR). Branched PEI of 1 kDa was bought from Polysciences, Inc. (Warrington, PA). Dialysis membrane tubing with a molecular weight cutoff (MWCO) of 0.5−1 kDa was purchased from Repligen (Waltham, Massachusetts).

2.2. Synthesis of FCDs. To synthesize polymeric F-CDs, various ratios of PEI to TFTA (1:3−10) were prepared.[29] Initially, TFTA, TA (for undoped fluorine carbon dots synthesis), and 1.8k PEI were combined in 15 mL of ethanol. Subsequently, the TFTA or TA and 1.8k b-PEI solutions were transferred to a Teflon-lined stainless-steel autoclave. Following thorough sonication, the solutions were heated for 6 h at 180 °C. The autoclave was then allowed to cool down to room temperature. The resulting products underwent dialysis using 1 kDa dialysis tubes. Finally, the synthesized F-CDs were freeze-dried for further characterization and experiments.

2.3. Structural Characterization. Transmission electron microscopy (JEOL JEM-3200FS) was utilized to characterize the morphology and size of F-CDs. Particle sizes were measured using ImageJ, and a histogram was plotted to depict the CDs' size distribution. Their average particle size and ζ-potential were measured with a Zetasizer ZSU3200 (Malvern Instruments, Inc., Worcestershire, U.K.). Fourier transform infrared (FT-IR) spectra were obtained using an Agilent Cary 630, while X-ray photoelectron spectroscopy (XPS) analysis was performed on a ThermoFisher Nexsa G2 X-ray photoelectron spectrometer with an Al source. The measurements were captured using a 400 μm spot size, complemented by a flood gun to correct any effects of charging. Survey scans were performed at a consistent pass energy of 200 eV, utilizing an energy step size of 1 eV across 1361 steps. The Avantage software (ThermoFisher 1999−2023, v6.6.1 Build 00029) facilitated the processing, analysis, and identification of peaks. Energy dispersive spectroscopy (EDS) experiments were conducted using the HITACHI SU 3500 microscope, with carbon tape utilized as the substrate for sample analysis. The accelerating voltage ranged from 10 to 15 kV. X-ray diffraction (XRD) analyses were conducted with 2θ values between 5 and 90° using a Bruker D8 Venture, equipped with a

https://doi.org/10.1021/acsanm.4c03109
ACS Appl. Nano Mater. 2024, 7, 21410−21419

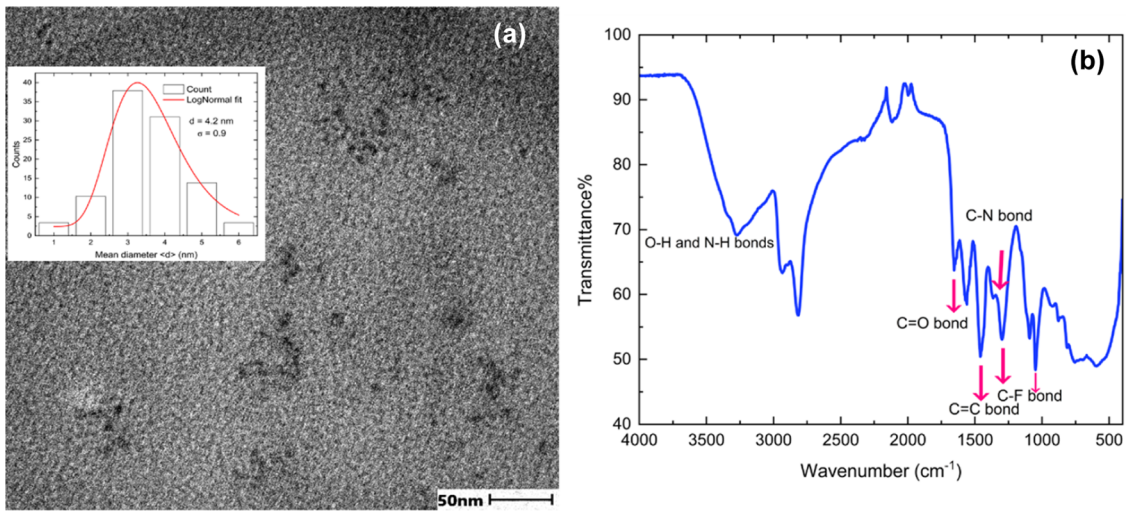

Figure 2. TEM image of the F-CDs at 50 nm scale, the inset represents the size distribution of F-CD (a). FT-IR spectrum of F-CD (b).

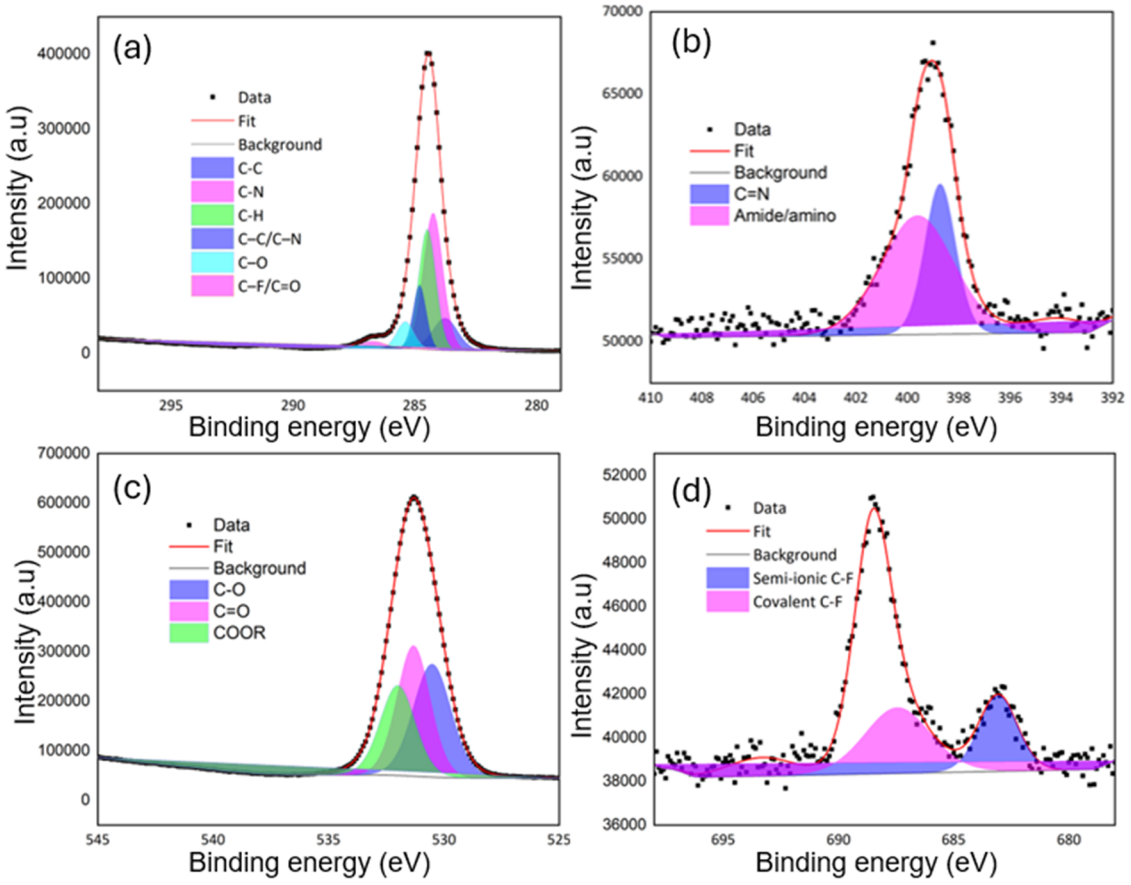

Figure 3. High-resolution XPS spectra of synthesized F-CDs. The elemental scans of the FCD flow as C 1s (a), N 1s (b), O 1s (c), and F 1s (d).

dual-wavelength X-ray source (high-intensity copper and molybdenum sources) and a revolutionary air-cooled PHOTON II CPAD detector. The ^{19}F NMR spectra were acquired using a 400 MHz Avance-III spectrometer (Bruker) with D_2O as the solvent. The luminescence and ultraviolet−visible (UV−vis) absorption measurements of the samples were conducted using an FL 6500 and UV−vis Lambda 365+ (PerkinElmer), respectively.

2.4. QY Measurement. Quinine sulfate (QY = 0.54) is a quantum yield reference that can be used to find the QY of each prepared fluorescent carbon dot. Five μM Quinine sulfate was dissolved in 0.1 M sulfuric acid (98%) (η = 1.33), whereas CDs were dissolved in ultrapure water with a refractive index (η) of 1.33. Next, using λ_{ex} = 345 nm, the fluorescence emission of these sample solutions from 350 to 650 nm was analyzed. After comparing the integrated fluorescence intensities (excited at 345 nm) and absorbance values (below 0.15 at 345 nm) of CDs with quinine sulfate.

2.5. Procedure for Detecting PFOA. The assay for detecting PFOA was set up by preparation of F-CDs solution at specific concentrations (0.44 mg/mL F-CDs). Different concentrations of PFOA were then added to this solution, followed by incubation at 25 °C for 30 min. Right after, fluorescence emission spectra (λ_{ex} = 350

https://doi.org/10.1021/acsanm.4c03109
ACS Appl. Nano Mater. 2024, 7, 21410−21419

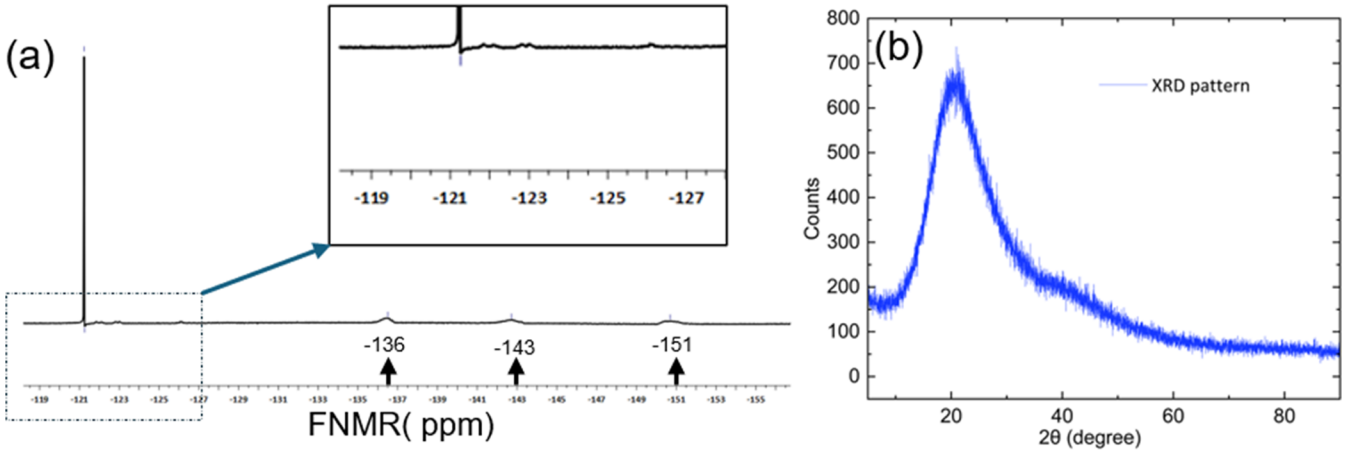

Figure 4. ^{19}FNMR spectrum of F-CD (a), XRD image of F-CDs (b).

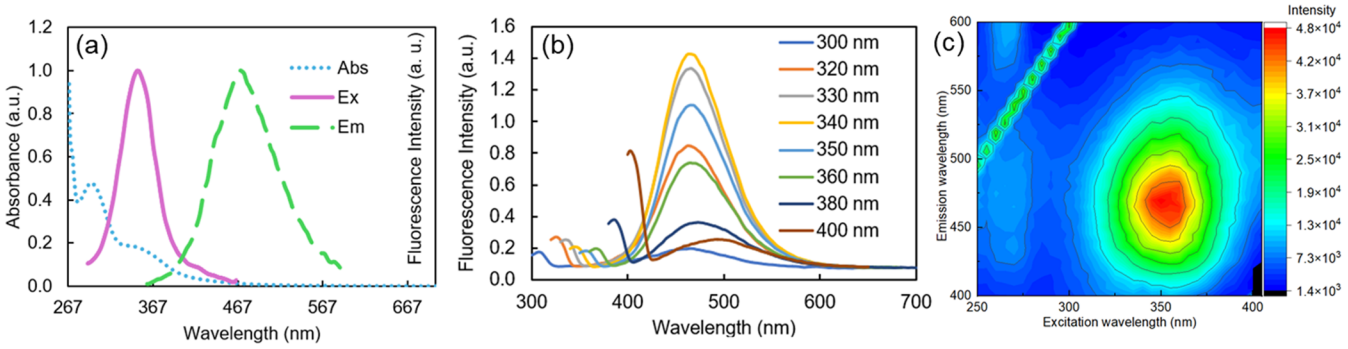

Figure 5. Normalized UV−vis absorption, FL excitation (λ_{em} = 465 nm), and FL emission (λ_{ex} = 350 nm) spectra of the F-CDs in DI water (a), Fluorescence spectra of F-CDs under different excitation wavelengths and (b) the corresponding counter map of 0.44 mg mL^{-1} F-CDs in DI water (c).

nm) were recorded for quantitative analysis (Excitation slit 5 nm, Emission slit 5 nm, and voltage 350 V). For this turn-on sensor, ΔF was defined as $F - F_0$, where F and F_0 are the fluorescence intensities of the F-CDs solutions with and without PFOA, respectively. For the standard addition recovery tests, groundwater samples were first boiled, allowed to cool down to room temperature, and then filtered three times using a 0.22 μm filter membrane.

3. RESULTS AND DISCUSSION

3.1. Properties of F-CDs. Polyethylenimine-based fluorinated carbon dots (PEI-F-CDs) were produced using a solvothermal method in which branched PEI and TFTA were reacted in an autoclave reactor (see Figure 1). In this process, TFTA was used as a cross-linker and the aromatic fluorine source, which mediates condensation reactions between its carboxyl groups and the amine groups of PEI.[29] The yellow suspension as a resultant was subjected to lyophilization, which produced approximately 175.4 mg for 1 mL of the F-CDs product. In the synthesis of polymeric F-CDs, two ratios of PEI to TFTA (1:3 and 1:10) were tested and a higher proportion of the nitrogen moiety at a 1:3 ratio significantly enhanced the quantum yield of the CDs. Figure 2a displays the transmission electron microscopy (TEM) image of the synthesized F-CDs along with their size distribution histogram. The image revealed that the F-CDs were spherical and uniformly spread across the carbon-coated copper grid. The average diameter of the F-CDs was approximately 4.2 ± 0.9 nm, with sizes ranging from 1.0 to 6.0 nm, as shown in the inset of Figure 2a. Dynamic light scattering (DLS) analysis showed that the PEI-CDs have an average hydrodynamic diameter of 6.96 ± 0.44 nm (see Figure S1). Additionally, ζ-potential measurements revealed a positive charge (+18.57 ± 2.6 mV) (see Figure S2), likely attributed to the amine-rich nature of PEI. This observation was consistent with the expected outcome of the applied ratio of PEI to TFTA. The positive ζ-potential suggests that the nitrogen sites are partially protonated under these conditions. This also highlights the potential of F-CDs in PFAS detection applications.

Further, the chemical structure of F-CDs was investigated using FT-IR, XPS, EDS, XRD, and ^{19}F NMR techniques. The extent of transforming alkylamines to aromatic nitrogen during the solvothermal process requires further confirmation. The FT-IR spectrum indicated the presence of N−H and O−H bonds observed in the range from 3000 to 3600 cm^{-1}, C═O (1650 cm^{-1}), C═C (1460 cm^{-1}), C−N (1423 cm^{-1}), C−O (1094 cm^{-1}), C−F (1297 and 1050 cm^{-1}) bonds in the F-CDs (Figure 2b).[30−34] The stretching vibration of a characteristic peak C−H at 2740 cm^{-1} indicates that the F-CDs may contain methyl or methylene groups.

The chemical compositions of F-CDs were additionally analyzed using XPS. The full XPS profiles of the F-CDs (Figure S3) display four main peaks at 284, 398, 530, and 688 eV, which correspond to C 1s, N 1s, O 1s, and F 1s, respectively. The high-resolution spectrum of C 1s (Figure 3a) displayed four peaks at 283.6, 284.1, 284.5, 284.7, 285.3, and 286.8 eV, corresponding to C−C, C−N, C−H, C−C/C−N, C−O, C−F/C═O bonds, respectively.[29,30,34] The high-resolution spectra of N 1s indicated the existence of C═N

https://doi.org/10.1021/acsanm.4c03109
ACS Appl. Nano Mater. 2024, 7, 21410−21419

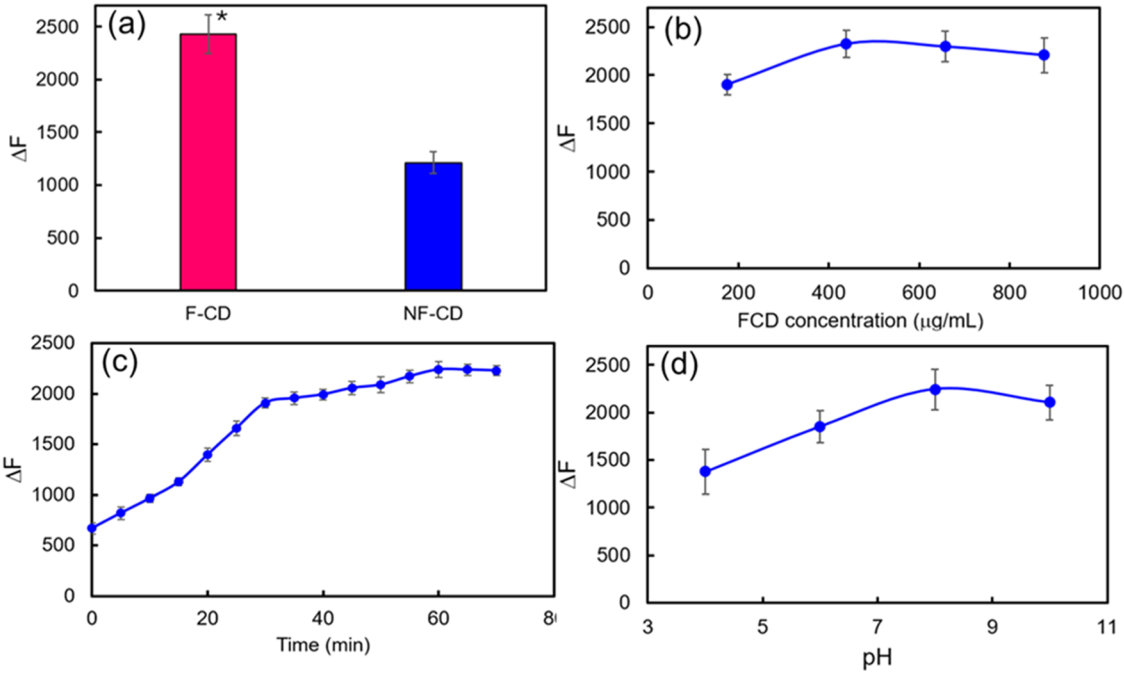

Figure 6. Comparison of fluorescence responses of F-CD and NF-CD to 0.5 ppb PFOA (a), Effect of the F-CDs concentration on the fluorescence intensity in the presence of PFOA (100 ppt) (b), Influence of reaction time on the fluorescence intensity of F-CDs with PFOA (c), Influence of pH on the fluorescence intensity of F-CDs with PFOA (d). The asterisk indicates the statistical differences.

bonds at 398.6 eV and amide/amino type N atoms at 399.6 eV (Figure 3b).[35] The high-resolution O 1s spectrum (Figure 3c) displays three peaks at 530.4, 531.2, and 532.0 eV, which correspond to C−O, C═O, and COOR groups, respectively.[34] The F 1s spectrum shown in Figure 3d displays two prominent peaks at 685.6 and 686.5 eV, corresponding to semi-ionic C−F and covalent C−F bonds, respectively. These fluorine bonds significantly enhance the interaction between the F-CDs and PFOA.[34] Multielement EDS mapping images (Figure S4a−d), along with the EDS spectrum of F-CDs, show detectable elements C, O, N, and F, with elemental percentages in the inset (Figure S4e). The elemental composition of F-CDs, as determined by EDS analysis, includes carbon at 55.9%, nitrogen at 34.7%, oxygen at 8.2%, and fluorine at 1.2%.

In addition, the presence of fluorine in synthesized FCDs was identified using the ^{19}F NMR spectra. As seen in Figure 4a, all the peaks fall between −160 and −100 in terms of chemical shift, which is consistent with indications of fluorine atoms attaching to aromatic rings. Based on the characterization and analysis as previously discussed, it is deduced that F-CDs consist of a carbonaceous core with multiple branched chains. These chains include aromatic fluorine groups and branched PEI segments, as illustrated in Figure 1.[17] The XRD pattern for the synthesized F-CDs, depicted in Figure 4b, shows a wide diffraction peak at 2θ = 20.9°, which is associated with the disordered carbon phase. The absence of sharp peaks in the XRD patterns indicates the existence of amorphous carbon.[36,37]

UV−Vis absorption and FL spectra were used to evaluate the optical properties of F-CDs. As shown in Figure 5a, F-CDs exhibit two characteristic absorption peaks at 295 and 355 nm, which can be assigned to $\pi-\pi^*$ (aromatic C═C) and $n-\pi^*$ (carboxyl C═O) transitions, respectively.[29] The inset photo in Figure 5a, displays the optical images of the aqueous F-CD dispersion under a UV lamp, illuminated by UV light at 365 nm. The optimal excitation and emission wavelengths are 350 and 465 nm, respectively. The F-CDs exhibited an excitation-dependent feature, with emission wavelengths ranging from 450 to 500 nm corresponding to excitations in the wavelength range of 300 to 400 nm (see Figure 5b). A corresponding contour plot for a 0.44 mg/mL CD solution in deionized water (DI) water, is depicted in Figure 5c. Fluorescence analysis demonstrated excitation/emission peaks at 350:465 nm, consistent with other PEI-based carbon dots, suggesting that the dots hold amorphous or polymeric nature.

The QY of C-dots was computed using the subsequent eq 1[38−40]

$$\phi_x = \phi_{st}(I_x/I_{st})(\eta_x^2/\eta_{st}^2)(A_{st}/A_x) \quad (1)$$

The subscript "s" denotes CDs, while the subscript "st" represents the standard substance. The terms ϕ_x, ϕ_{st}, I_x, I_{st}, η_x, η_{st}, A_x and A_{st} correspond to the QY, integrated fluorescence emission intensity, refractive index of the solvent intensity, absorbance of the sample, and quinine sulfate, respectively. As seen in Table S1, the highest quantum yield, reaching 10.6%, was obtained with a 1:3 ratio (PEI/TFTA), suggesting this is the most effective doping balance for increased sensitivity. This improvement is credited to the synergistic effects of N and F doping, which markedly enhanced the fluorescence quantum yield of the CDs.

3.2. Turn on Mechanism between F-CD and PFOA. ζ-Potential analysis was used to monitor the changes in the surface charge of F-CDs as interacted with PFOA. Initially, the F-CDs exhibited a ζ-potential of +18.57 ± 2.6 mV, indicating a positively charged probe. This positive charge could be attributed to the different amounts of protonated amine on F-CDs. The presence of PEI in the reaction system likely increased the proportion of protonated amine groups relative to other surface functional groups.[41] The calculated ζ-potential values for F-CDs before and after the introduction of PFOA

https://doi.org/10.1021/acsanm.4c03109
ACS Appl. Nano Mater. 2024, 7, 21410−21419

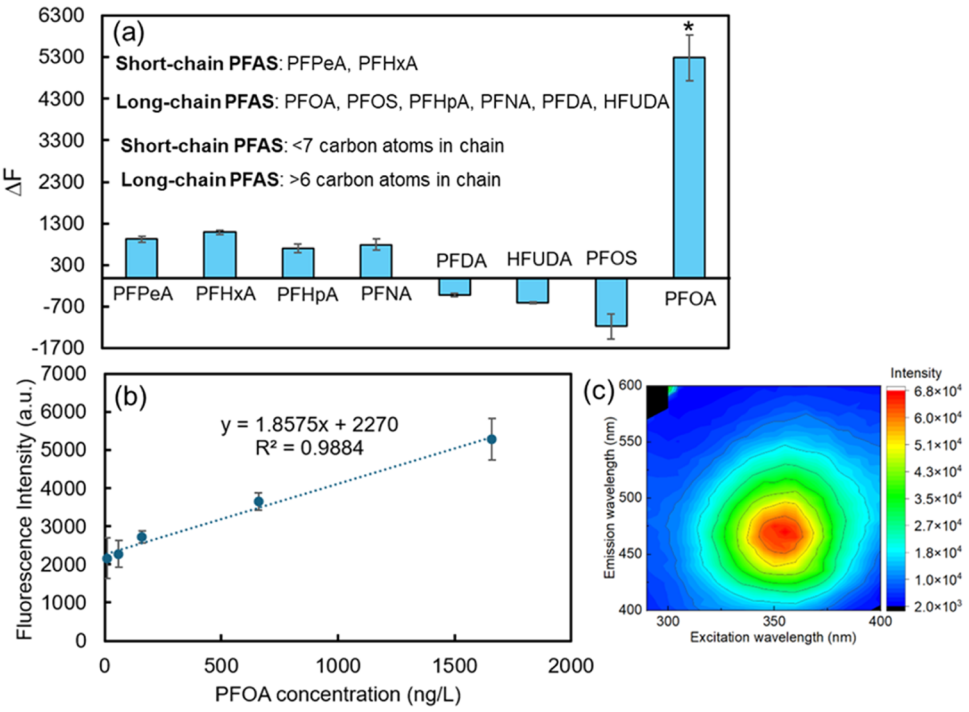

Figure 7. Fluorescence intensity enhanced the ΔF_{F-F0} value of the F-CDs in response to various perfluorinated compounds, with PFAS detected at 1.6 ppb and F-CD concentration at 0.44 mg/mL (a), The fluorimetry calibration curves for the determination of PFOA (b), corresponding counter map exposed to various concentrations of PFOA (c). The asterisk indicates the statistical differences.

align with the proposed mechanism. Notably, the ζ-potential of F-CDs decreased from +18.57 mV to +5.978 mV after biding with PFOA (200 ppt) (Figures S2 and S5). Fluorinated probes utilized the selective properties of fluorophilic interactions for targeted binding with PFAS.[11] As illustrated in Figure 6a, we compared the fluorescence responses of assays using F-CDs and CDs with no fluorine (NF-CDs). The fluorescence change observed with the F-CD-based sensor was significantly higher than that of the NF-CD-based sensor. This indicates that the interaction between F-CD and PFOA is driven by both electrostatic and fluorophilic interactions.

3.3. Optimization of the Assay. To attest the F-CDs performance over the detection of PFOA and optimize the influential factors, a series of studies were conducted including the effects of temperature, NaCl concentration, F-CD concentration, the influence of pH, and incubation time on the increase in fluorescence (results depicted in Figure 6b–d).

3.3.1. Effect of Temperature. The fluorescence intensity of F-CDs slightly decreased with increasing temperature, with the highest intensity observed at 20 °C and a gradual decline up to 50 °C (Figure S6). This trend is likely due to increased nonradiative decay processes at higher temperatures, which can quench fluorescence. Considering the negligible variation in fluorescence intensity observed between 20 and 30 °C, room temperature was selected as the optimal temperature to ensure the best balance between signal strength and stability.

3.3.2. Effect of NaCl Concentration. We tested the effect of different NaCl concentrations on the stability of the fluorescence signal by varying the concentration from 0.0005 to 0.05 M (Figure S7). The fluorescence intensity remained stable across all tested concentrations, indicating that the assay is robust and not significantly affected by changes in NaCl concentration.

3.3.3. Effect of F-CDs Concentration. The effect of F-CD concentration on fluorescence intensity in the presence of PFOA is illustrated in Figure 6b. Four different concentrations of F-CD—175.4, 438.5, 658, and 877 μg/mL—were evaluated in the presence of 100 ppt PFOA. The fluorescence intensity corresponded to the highest level of 438.5 μg/mL, indicating optimal interaction between F-CDs and PFOA. Beyond this concentration, particularly at 877 μg/mL, a decrease in fluorescence intensity was observed. This reduction is likely due to self-quenching, as suggested by the F-CDs at higher concentrations in literature.[42] Further experimental and theoretical analysis is required to fully elucidate this phenomenon.

3.3.4. Optimization of Reaction Time. The reaction time between the F-CDs and PFOA is a critical factor influencing the speed and sensitivity of the procedure. As shown in Figure 6c, the fluorescence intensity of the F-CDs was monitored in the presence of PFOA over a period of 0–70 min after thorough mixing under optimal conditions. The response increased with incubation time, reaching a maximum of 60 min, after which it remained constant, indicating that equilibrium had been achieved in the interaction between F-CDs and PFOA. Therefore, we extended the incubation time to 60 min for further experiments.

3.3.5. pH Optimization. The stability of the F-CDs was tested at a pH range from 5 to 10 (Figure S8). The fluorescence intensity remained almost the same at pH levels 6, 7, 8, 9, and 10, demonstrating the stability of the assay under different pH conditions. However, at pH 5, the fluorescence intensity increased slightly. This increase could be attributed to the protonation of functional groups on the F-CDs at lower pH. The turn-on fluorescence response ($\Delta F = F - F_0$) of cationic F-CDs at various pH values is shown in Figure 6d. Interestingly, despite the cationic F-CDs being more positively

https://doi.org/10.1021/acsanm.4c03109
ACS Appl. Nano Mater. 2024, 7, 21410–21419

Table 1. Comparison with Other Assays for PFOA Detection, Emphasizing That None Required a Preconcentration Step Prior to Measurement

methods	nanomaterials	LOD	linear range	refs
electrochemical sensing	AuNPs	24 ppt	100−5000 ppt	45
fluorescence sensor		70 ppb	-	46
photoluminescence	core−shell quantum dots	10.4 ppb	103.5−6211 ppb	47
fluorescence sensor	CdS quantum dot	0.12 ppm	0.2−16.5 ppm	42
fluorescence sensor	CdTe quantum dot	19.78 ppt	19.8−2070 ppt	48
fluorescence sensor	carbon quantum dots (CQDs)	4.14 ppb	41.4−621.1 ppb	26
fluorescence sensor	Se, N codoped CQDs	0.74 ppm	4.1−29.0 ppm	27
optical fiber sensor	graphene oxide	0.4 ppb	0−2 ppb	8
bacterial biosensor		10 ppt	10−1000 ppt	49

Table 2. Measuring PFOA in El Paso Well and Tap Water Samples, with Each Experiment Conducted in Triplicate to Ensure the Reproducibility of the Results

samples	found (ppt)	spiked (ppt)	detected (ppt)	recovery%	RSD%
well water	0.0	10.0	10.6, 9.9, 9.8	106.0, 99.0, 98.0	6.8
		60.0	55.2, 62.3, 58.4	92.0, 104.0, 97.3	6.1
		160.0	152.4, 152.7,157.6	95.3, 95.4, 98.5	1.9
tap Water	0.0	10.0	9.99, 10.5, 10.3	99.9, 105.0, 103.0	2.5
		60.0	59.96, 60.7, 60.3	99.9, 101.2, 100.5	0.6
		160.0	165.0, 154.1, 162.5	103.1, 96.3, 101.6	3.6

charged at pH 4, according to ζ-potential (measure 45 mV), the response is stronger at higher pH values (6, 8, and 10). At higher pH values, the interaction between cationic carbon dots and PFOA is more effective. At these pH levels, the improved dispersion of F-CDs facilitates better access to their surface sites for PFOA binding. This pH-dependent behavior is crucial for optimizing the conditions for sensitive and effective detection of PFOA using cationic F-CDs.[25,43] Moreover, pH levels in water resources fall within 5 to 8, where 99% of PFOA exists in its ionized form, dictating a behavior that is largely influenced by the characteristics of the anion.[44] This ionization enhances the interaction between the negatively charged PFOA and the cationic F-CD, particularly at higher pH levels where the F-CDs are more effectively dispersed. This led to a more significant "turn-on" fluorescence response in this pH range. pH 8 was chosen as the optimal pH, as the fluorescence difference (ΔF) was higher than at pH 6 and 10, indicating a stronger and more reliable response at this condition.

3.3.6. Selectivity of the Assay for PFOA Determination. To investigate the specificity of the fluorescent F-CDs, a variety of perfluorinated substances, including perfluorooctanesulfonic acid (PFOS), perfluoropentanoic acid (PFPeA), perfluorohexanoic acid (PFHxA), perfluoroheptanoic acid (PFHpA), perfluorononanoic acid (PFNA), perfluorodecanoic acid (PFDA), and henicosafluoroundecanoic acid (HFUDA) were introduced into the reaction environment instead of PFOA under ideal conditions. As depicted in Figure 7a, PFOA uniquely induced a significant enhancement in the fluorescence intensity of the F-CDs, whereas the other compounds showed negligible influence. Figure S9 shows the enhanced fluorescence intensity (ΔF) of F-CDs in response to various possible interfering substances, with PFOA detected at a concentration of 1.6 ppb and inorganic chemicals at 3.0 mg/mL. Figure S9 demonstrates that these substances had a negligible effect on PFOA detection. This demonstrates the excellent specificity of the fluorescent F-CDs toward PFOA.

3.4. Analytical Parameters. To assess the sensitivity of the method for detecting PFOA, varying concentrations ranging from 10 to 1660 ppt were introduced into the sensing system under optimized conditions. Figure 7b illustrates the calibration curve, generated by plotting the increase in fluorescence intensity ΔF ($F - F_0$) against the PFOA concentration (cPFOA). The linear regression formula obtained is $\Delta F = 1.8575(\text{cPFOA}) + 2270$, with a correlation coefficient of 0.9884, indicating linear responses to PFOA at concentrations between 10 and 1660 ppt. Following established methodologies, $3\sigma/s$ was used to determine the detection limit (LOD), which was found to be 3 ppt using fluorimetry, highlighting the method's high sensitivity. Additionally, when compared with other techniques for PFOS analysis listed in Table 1, this method's detection limit is either comparable or lower.[8,26,27,42,45−49] Unlike more complex methods, this approach is straightforward, cost-effective, and does not require preconcentration, utilizing an affordable instrument. Thus, it proves to be an effective tool for PFOA detection.

3.5. Analytical Application. The practical viability of the fluorescence probe was tested using random groundwater samples from El Paso, Texas. The initial experiments indicated that PFOA was undetectable in both tap and groundwater. Consequently, the standard addition method was utilized for evaluating these real water samples. The sample processing involved two phases, where initially the water samples were boiled and then allowed to cool down to room temperature. Subsequently, samples were filtered three times through a 0.22 μm filter membrane, with this process being repeated three times. As detailed in Table 2, three low concentrations of PFOA were added to the samples ($n = 3$). Recovery rates for these standard additions were between 92 and 106%, with relative standard deviations (RSD) of less than 6.8%. These findings support the use of the fluorescence probe for the detection of PFOA in actual water samples.

4. CONCLUSIONS

In conclusion, a nanoscale fluorescence probe using engineered fluorinated carbon dots was designed for the detection of

https://doi.org/10.1021/acsanm.4c03109
ACS Appl. Nano Mater. 2024, 7, 21410−21419

PFAS in aqueous systems, targeting PFOA as a marker for the extent of PFAS contamination. The ratio of N/F was optimized and extensively characterized using NMR, XRD, XPS and FTIR. The use of PEI in synthesizing F, N-CDs resulted in positively charged nanoscale F-CDs with an average diameter of 4.2 nm. The characterization of the F-CDs and their operation provided strong evidence as the primary turn-on mechanisms is driven by electrostatic and fluorophilic interactions between the negatively charged PFOA and positively charged F-CDs. The selectivity of this method toward PFOA detection was further tested with seven more PFAS analytes. The sensor showed high sensitivity for PFOA, with a detection range of 10−1660 ppt and a low detection limit of 3 ppt. The sensor's applicability was evaluated using groundwater samples contaminated with PFAS. Above all, the methos is comparable to many recently developed methods. Further, it stands out among available methods due to its reliability, simplicity, cost-effectiveness, and eliminating the need for complex modifications. The Density Functional Theory (DFT) calculations can provide deeper insights into the electronic properties and interactions of F-CDs with PFAS molecules. Further, synthesizing hybrid nanostructures by combining F-CDs with other materials, such as metal nanoparticles or MOFs, can synergistically enhance detection capabilities. This work not only contributes to the field of environmental monitoring but also opens new avenues for the development of highly sensitive and selective sensors for various PFAS molecules, thereby safeguarding water resources and public health.

■ ASSOCIATED CONTENT

Supporting Information

The Supporting Information is available free of charge at https://pubs.acs.org/doi/10.1021/acsanm.4c03109.

F-CD average particle size (Figure S1); F-CD ζ-potential (Figure S2); F-CDs XPS survey spectrum (Figure S3); multielement EDS mapping images (Figure S4); calculated quantum yield (Table S1); F-CD ζ-potential after adding PFOA (Figure S5); effect of temperature (Figure S6); effect of NaCl concentration (Figure S7); effect of pH (Figure S8); ΔF of F-CDs in response to inorganic contaminants (Figure S9) (PDF)

■ AUTHOR INFORMATION

Corresponding Authors

Somayeh Mohammadi − *Department of Chemistry and Biochemistry, University of Texas at El Paso, El Paso, Texas 79968, United States*; Email: smohammadi1@miners.utep.edu

Hamidreza Sharifan − *Department of Chemistry and Biochemistry, University of Texas at El Paso, El Paso, Texas 79968, United States*; orcid.org/0000-0002-6990-0635; Email: hsharifan@utep.edu

Author

Zayra N. Dorado − *Department of Metallurgical & Materials Engineering, The University of Texas at El Paso, El Paso, Texas 79902, United States*

Complete contact information is available at: https://pubs.acs.org/10.1021/acsanm.4c03109

Notes

The authors declare no competing financial interest.

■ ACKNOWLEDGMENTS

We acknowledge the Agriculture and Food Research Initiative (AFRI) Competitive Grant by National Institute of Food and Agriculture (NIFA), United State Department of Agriculture (USDA), grant #2024-67022-42827 within the program code A1511. We thank Dr. Wen-Yee Lee for providing environmental samples and chemicals. We are grateful to Dr. Dino Villagran's Lab, Dr. Xiujun (James) Li, Dr. Metta, Dr. Ramos, and Dr. Sohan De Silva for their facility support. The XPS system was funded by NSF/CHEM grant 2216473.

■ REFERENCES

(1) Kidd, J.; Fabricatore, E.; Jackson, D. Current and future federal and state sampling guidance for per-and polyfluoroalkyl substances in environmental matrices. *Sci. Total Environ.* **2022**, *836*, No. 155523.

(2) Sharifan, H.; Bagheri, M.; Wang, D.; Burken, J. G.; Higgins, C. P.; Liang, Y.; Liu, J.; Schaefer, C. E.; Blotevogel, J. Fate and transport of per-and polyfluoroalkyl substances (PFASs) in the vadose zone. *Sci. Total Environ.* **2021**, *771*, No. 145427.

(3) Young, R. B.; Pica, N. E.; Sharifan, H.; Chen, H.; Roth, H. K.; Blakney, G. T.; Borch, T.; Higgins, C. P.; Kornuc, J. J.; McKenna, A. M.; Blotevogel, J. PFAS analysis with ultrahigh resolution 21T FT-ICR MS: suspect and nontargeted screening with unrivaled mass resolving power and accuracy. *Environ. Sci. Technol.* **2022**, *56* (4), 2455−2465.

(4) Garg, A.; Shetti, N. P.; Basu, S.; Nadagouda, M. N.; Aminabhavi, T. M. Treatment technologies for removal of per-and polyfluoroalkyl substances (PFAS) in biosolids. *Chem. Eng. J.* **2023**, *453*, No. 139964.

(5) Mann, M. M.; Berger, B. W. A genetically-encoded biosensor for direct detection of perfluorooctanoic acid. *Sci. Rep.* **2023**, *13* (1), No. 15186.

(6) Feng, Y.; Dai, J.; Wang, C.; Zhou, H.; Li, J.; Ni, G.; Zhang, M.; Huang, Y. Ag Nanoparticle/Au@ Ag Nanorod Sandwich Structures for SERS-Based Detection of Perfluoroalkyl Substances. *ACS Appl. Nano Mater.* **2023**, *6* (15), 13974−13983.

(7) Sharma, S.; Shetti, N. P.; Basu, S.; Nadagouda, M. N.; Aminabhavi, T. M. Remediation of per-and polyfluoroalkyls (PFAS) via electrochemical methods. *Chem. Eng. J.* **2022**, *430*, No. 132895.

(8) Faiz, F.; Cran, M. J.; Zhang, J.; Muthukumaran, S.; Sidiroglou, F. Graphene Oxide Doped Alginate Coated Optical Fiber Sensor for the Detection of Perfluorooctanoic Acid in Water. *IEEE Sens. J.* **2023**, *23* (12), 12861−12867.

(9) McMahon, P. B.; Tokranov, A. K.; Bexfield, L. M.; Lindsey, B. D.; Johnson, T. D.; Lombard, M. A.; Watson, E. Perfluoroalkyl and polyfluoroalkyl substances in groundwater used as a source of drinking water in the eastern United States. *Environ. Sci. Technol.* **2022**, *56* (4), 2279−2288.

(10) Ganesan, S.; Chawengkijwanich, C.; Gopalakrishnan, M.; Janjaroen, D. Detection methods for sub-nanogram level of emerging pollutants−Per and polyfluoroalkyl substances. *Food Chem. Toxicol.* **2022**, *168*, No. 113377.

(11) Wang, Y.; Darling, S. B.; Chen, J. Selectivity of per-and polyfluoroalkyl substance sensors and sorbents in water. *ACS Appl. Mater. Interfaces* **2021**, *13* (51), 60789−60814.

(12) Breshears, L. E.; Mata-Robles, S.; Tang, Y.; Baker, J. C.; Reynolds, K. A.; Yoon, J.-Y. Rapid, sensitive detection of PFOA with smartphone-based flow rate analysis utilizing competitive molecular interactions during capillary action. *J. Hazard. Mater.* **2023**, *446*, No. 130699.

(13) Mohammadi, S.; Mohammadi, S.; Salimi, A.; Ahmadi, R. A chelation-enhanced fluorescence assay using thiourea capped carbonaceous fluorescent nanoparticles for As (III) detection in water samples. *J. Fluoresc.* **2022**, *32*, 145−153.

(14) Pirsaheb, M.; Mohammadi, S.; Khodarahmi, R.; Hoseinkhani, Z.; Mansouri, K.; Payandeh, M. A turn off fluorescence probe based on carbon dots for highly sensitive detection of BRCA1 gene in real samples and cellular imaging. *J. Fluoresc.* **2022**, *32* (5), 1733−1741.
(15) Caroleo, F.; Magna, G.; Naitana, M. L.; Di Zazzo, L.; Martini, R.; Pizzoli, F.; Muduganti, M.; Lvova, L.; Mandoj, F.; Nardis, S.; et al. Advances in optical sensors for persistent organic pollutant environmental monitoring. *Sensors* **2022**, *22* (7), No. 2649.
(16) Lu, Y.; Xia, X.; Guo, Y.; Sun, C.; Ma, J.; Wang, Q. Carbon Dots/SiO2 Fluorescent Photonic Crystals for Anti-Counterfeiting. *ACS Appl. Nano Mater.* **2024**, *7* (6), 6547−6555.
(17) Lewis, R. E.; Huang, C.-H.; White, J. C.; Haynes, C. L. Using 19F NMR to Investigate Cationic Carbon Dot Association with Per- and Polyfluoroalkyl Substances (PFAS). *ACS Nanosci. Au* **2023**, *3* (5), 408−417.
(18) Murugan, K.; Jothi, V. K.; Rajaram, A.; Natarajan, A. Novel metal-free fluorescent sensor based on molecularly imprinted polymer N-CDs@ MIP for highly selective detection of TNP. *ACS Omega* **2022**, *7* (1), 1368−1379.
(19) Mohammadi, S.; Salimi, A. Fluorometric determination of microRNA-155 in cancer cells based on carbon dots and MnO 2 nanosheets as a donor-acceptor pair. *Microchim. Acta* **2018**, *185*, No. 372.
(20) Gruber, A.; Navarro, L.; Klinger, D. Reactive precursor particles as synthetic platform for the generation of functional nanoparticles, nanogels, and microgels. *Adv. Mater. Interfaces* **2020**, *7* (5), No. 1901676.
(21) RSantiago, A. R.; Yin, S.; Elbert, J.; Lee, J.; Shukla, D.; Su, X. Imparting selective fluorophilic interactions in redox copolymers for the electrochemically mediated capture of short-chain perfluoroalkyl substances. *J. Am. Chem. Soc.* **2023**, *145* (17), 9508−9519.
(22) Xiao, L.; Ling, Y.; Alsbaiee, A.; Li, C.; Helbling, D. E.; Dichtel, W. R. *β*-Cyclodextrin polymer network sequesters perfluorooctanoic acid at environmentally relevant concentrations. *J. Am. Chem. Soc.* **2017**, *139* (23), 7689−7692.
(23) Tan, X.; Sawczyk, M.; Chang, Y.; Wang, Y.; Usman, A.; Fu, C.; Král, P.; Peng, H.; Zhang, C.; Whittaker, A. K. Revealing the molecular-level interactions between cationic fluorinated polymer sorbents and the major PFAS pollutant PFOA. *Macromolecules* **2022**, *55* (3), 1077−1087.
(24) Wan, H.; Fang, F.; Shi, K.; Yi, Z.; Lei, L.; Li, S.; Mills, R.; Bhattacharyya, D.; Xu, Z. pH-Swing membrane adsorption of perfluoroalkyl substances: Anion-exchange brushes and role of water chemistry. *Sep. Purif. Technol.* **2024**, *329*, No. 124800.
(25) Lin, L.; Zhou, S.; Guo, H.; Chen, Y.; Lin, S.; Yan, L.; Li, K.; Li, J. Nitrogen-doped carbon dots as an effective fluorescence enhancing system for the determination of perfluorooctyl sulfonate. *Microchim. Acta* **2019**, *186*, No. 380.
(26) Hong, Y.; Chen, X.; Zhang, Y.; Zhu, Y.; Sun, J.; Swihart, M. T.; Tan, K.; Dong, L. One-pot hydrothermal synthesis of high quantum yield orange-emitting carbon quantum dots for sensitive detection of perfluorinated compounds. *New J. Chem.* **2022**, *46* (41), 19658−19666.
(27) Walekar, L. S.; Zheng, M.; Zheng, L.; Long, M. Selenium and nitrogen co-doped carbon quantum dots as a fluorescent probe for perfluorooctanoic acid. *Microchim. Acta* **2019**, *186*, No. 278.
(28) Chen, Q.; Zhu, P.; Xiong, J.; Gao, L.; Tan, K. A sensitive and selective triple-channel optical assay based on red-emissive carbon dots for the determination of PFOS. *Microchem. J.* **2019**, *145*, 388−396.
(29) Zuo, G.; Xie, A.; Pan, X.; Su, T.; Li, J.; Dong, W. Fluorine-doped cationic carbon dots for efficient gene delivery. *ACS Appl. Nano Mater.* **2018**, *1* (5), 2376−2385.
(30) Wu, X.; Xu, M.; Wang, S.; Abbas, K.; Huang, X.; Zhang, R.; Tedesco, A. C.; Bi, H. F, N-Doped carbon dots as efficient Type I photosensitizers for photodynamic therapy. *Dalton Trans.* **2022**, *51* (6), 2296−2303.
(31) Zuo, W.; Tang, L.; Xiang, J.; Ji, R.; Luo, L.; Rogée, L.; Ping Lau, S. Functionalization of graphene quantum dots by fluorine: Preparation, properties, application, and their mechanisms. *Appl. Phys. Lett.* **2017**, *110* (22), No. 221901.
(32) Wang, J.; Hu, X.; Ding, H.; Huang, X.; Xu, M.; Li, Z.; Wang, D.; Yan, X.; Lu, Y.; Xu, Y.; et al. Fluorine and Nitrogen Co-Doped Carbon Dot Complexation with Fe (III) as a T 1 Contrast Agent for Magnetic Resonance Imaging. *ACS Appl. Mater. Interfaces* **2019**, *11* (20), 18203−18212.
(33) Zuo, G.; Xie, A.; Li, J.; Su, T.; Pan, X.; Dong, W. Large emission red-shift of carbon dots by fluorine doping and their applications for red cell imaging and sensitive intracellular Ag+ detection. *J. Phys. Chem. C* **2017**, *121* (47), 26558−26565.
(34) Hua, J.; Hua, P.; Qin, K. Highly fluorescent N, F co-doped carbon dots with tunable light emission for multicolor bio-labeling and antibacterial applications. *J. Hazard. Mater.* **2023**, *459*, No. 132331.
(35) Long, P.; Feng, Y.; Cao, C.; Li, Y.; Han, J.; Li, S.; Peng, C.; Li, Z.; Feng, W. Self-protective room-temperature phosphorescence of fluorine and nitrogen codoped carbon dots. *Adv. Funct. Mater.* **2018**, *28* (37), No. 1800791.
(36) Liu, Y.; Zhou, Q.; Yuan, Y.; Wu, Y. Hydrothermal synthesis of fluorescent carbon dots from sodium citrate and polyacrylamide and their highly selective detection of lead and pyrophosphate. *Carbon* **2017**, *115*, 550−560.
(37) Bajpai, S. K.; D'souza, A.; Suhail, B. Blue light-emitting carbon dots (CDs) from a milk protein and their interaction with Spinacia oleracea leaf cells. *Int. Nano Lett.* **2019**, *9*, 203−212.
(38) Zhou, X.; Zhao, G.; Tan, X.; Qian, X.; Zhang, T.; Gui, J.; Yang, L.; Xie, X. Nitrogen-doped carbon dots with high quantum yield for colorimetric and fluorometric detection of ferric ions and in a fluorescent ink. *Microchim. Acta* **2019**, *186*, No. 67.
(39) Chen, Q.; Zhu, P.; Xiong, J.; Gao, L.; Tan, K. A new dual-recognition strategy for hybrid ratiometric and ratiometric sensing perfluorooctane sulfonic acid based on high fluorescent carbon dots with ethidium bromide. *Spectrochim. Acta, Part A* **2020**, *224*, No. 117362.
(40) Liu, P.; Zhang, C.; Liu, X.; Cui, P. Preparation of carbon quantum dots with a high quantum yield and the application in labeling bovine serum albumin. *Appl. Surf. Sci.* **2016**, *368*, 122−128.
(41) Verma, A.; Arshad, F.; Ahmad, K.; Goswami, U.; Samanta, S. K.; Sahoo, A. K.; Sk, M. P. Role of surface charge in enhancing antibacterial activity of fluorescent carbon dots. *Nanotechnology* **2020**, *31* (9), No. 095101.
(42) Liu, Q.; Huang, A.; Wang, N.; Zheng, G.; Zhu, L. Rapid fluorometric determination of perfluorooctanoic acid by its quenching effect on the fluorescence of quantum dots. *J. Lumin.* **2015**, *161*, 374−381.
(43) Liang, Q.; Ma, W.; Shi, Y.; Li, Z.; Yang, X. Easy synthesis of highly fluorescent carbon quantum dots from gelatin and their luminescent properties and applications. *Carbon* **2013**, *60*, 421−428.
(44) Burns, D. C.; Ellis, D. A.; Li, H.; McMurdo, C. J.; Webster, E. Experimental p K a determination for perfluorooctanoic acid (PFOA) and the potential impact of p K a concentration dependence on laboratory-measured partitioning phenomena and environmental modeling. *Environ. Sci. Technol.* **2008**, *42* (24), 9283−9288.
(45) Solís, J. J. C.; Yin, S.; Galicia, M.; Ersan, M. S.; Westerhoff, P.; Villagrán, D. Forever chemicals" detection: A selective nano-enabled electrochemical sensing approach for perfluorooctanoic acid (PFOA). *Chem. Eng. J.* **2024**, No. 151821.
(46) Park, J.; Yang, K.-A.; Choi, Y.; Choe, J. K. Novel ssDNA aptamer-based fluorescence sensor for perfluorooctanoic acid detection in water. *Environ. Int.* **2022**, *158*, No. 107000.
(47) Zheng, L.; Zheng, Y.; Liu, Y.; Long, S.; Du, L.; Liang, J.; Huang, C.; Swihart, M. T.; Tan, K. Core-shell quantum dots coated with molecularly imprinted polymer for selective photoluminescence sensing of perfluorooctanoic acid. *Talanta* **2019**, *194*, 1−6.
(48) Zhang, F.; Liang, J.; Liu, Y.; Zhou, Q.; Hong, Y.; Chen, X.; Tan, K. A highly sensitive dual-readout assay for perfluorinated compounds based CdTe quantum dots. *Spectrochim. Acta, Part A* **2022**, *269*, No. 120753.

https://doi.org/10.1021/acsanm.4c03109
ACS Appl. Nano Mater. 2024, 7, 21410−21419

(49) Sunantha, G.; Vasudevan, N. A method for detecting perfluorooctanoic acid and perfluorooctane sulfonate in water samples using genetically engineered bacterial biosensor. *Sci. Total Environ.* **2021**, *759*, No. 143544.

https://doi.org/10.1021/acsanm.4c03109
ACS Appl. Nano Mater. 2024, 7, 21410−21419